JOURNAL OF MATERIALS SCIENCE **35** (2000) 5741–5749

# The use of digital images to determine deformation throughout a microstructure

## Part I *Deformation mapping technique*

C. M. NEUBAUER*
*Department of Materials Science, Northwestern University, Evanston, IL 60208, USA*
E. J. GARBOCZI
*National Institute of Standards and Technology, Gaithersburg, MD 20899, USA*
H. M. JENNINGS
*Departments of Materials Science and Civil Engineering, Northwestern University, Evanston, IL 60208, USA*
*E-mail: h-jennings@nwu.edu*

Materials with heterogeneous microstructures do not deform uniformly under stress (mechanical or environmental). A new deformation mapping technique (DMT), which compares digital images of microstructures of the same field of view before and after deformation occurs, is reported. Two digital images are required: a reference image, taken before deformation; and a deformed image, taken after deformation. The displacements of pixels required to match the deformed image to the reference image are computed, and these displacements are used to calculate the percent deformation in the two principal directions. Results are presented as either a deformation map, as a histogram, or as data files containing the displacements at the corner of each pixel. Comparison with exact solutions generated on a simulated microstructure shows that the accuracy of this technique is quite good. © *2000 Kluwer Academic Publishers*

## 1. Introduction

Although a material that undergoes mechanical deformation may appear at the macroscale to be deformed uniformly, at the microscale this is not the case, especially in multi-phase materials. It is the local deformations occurring within the microstructure that ultimately lead to cracking and failure. Some types of deformation, such as drying shrinkage in cement-based materials, involve complex processes at the micrometer and smaller levels, and they cannot be investigated directly without measuring displacement at this level.

One of the biggest problems in measuring deformations on the microscale is that the displacements involved are too small to be measured easily or accurately. However, a recent paper has described an image intensity matching technique (IIMT) capable of detecting very small *displacements* of features in digital images [1]. This technique uses a minimum mean square error criterion to compare a *reference* image, taken before deformation, and a *deformed* image, taken after a stress of some kind is applied to the sample and deformation occurs. Displacements can be determined with a resolution of approximately ±0.2 pixels. Since the IIMT operates on the pixel gray levels of each image, the source of the digital images is irrelevant, and the source of the deformation may include mechanical, thermal, and/or environmental stress.

Though the magnitude of deformations between several pairs of points due to drying shrinkage in the cement paste microstructure has been previously determined [2–4], no information about the actual physical distribution of deformation within the microstructure was presented. The spatial distribution of deformation could provide more valuable information than can be expressed in a single number like the average overall drying shrinkage. For example, certain mechanisms may be masked if the large-scale deformation alone is studied, because although it may appear that little overall deformation occurred, there still may be fairly large micro-scale tensile and compressive mechanisms that balanced each other, resulting in a low net deformation. Furthermore, in composite materials with important internal interfaces, concentrations of deformation may dominate behavior.

This paper outlines a new deformation mapping technique (DMT) capable of providing a physical representation of the deformations in a microstructure. Because this technique is based on the IIMT mentioned previously, the DMT will also work on any set of digital images. The DMT takes the displacements computed

---

* *Present Address*: Valspar Corporation, Pittsburgh, PA 15233, USA.

by the IIMT and then uses a finite element interpolation technique to compute deformations, averaged from the principal deformations over each pixel. A description of this technique, and the information that can be extracted from it, are presented in the following section. Image resolution and the effects of scale on the DMT are also discussed.

As with any microscopic technique or any surface strain measuring technique, information is obtained from a surface, and results must be interpreted accordingly. In particular, a free surface is not as constrained as the interior, and associated deformations will be different than they are beneath the surface. Nevertheless, new insights can be obtained using the DMT.

## 2. Deformation vs. strain

It is important to differentiate between deformation and elastic strain for the following analysis. Deformation is analogous to elastic strain, as both can be defined as the limit of the change in length over the initial length, as the initial length goes to zero.

Elastic strain, either in the linear limit of small strains [5], or in the more general finite strain regime [6, 7], implies that the stress state can be determined by multiplying by the appropriate modulus. However, drying shrinkage is a highly inelastic situation, with a large viscoelastic component. De-bonding can occur and rearrangement of phases is possible, which can result in unusually large local displacements. Thus, while the deformations within the microstructure are computed from the displacements using a finite strain formulation (see Section 3.3), they cannot be related directly to a stress state as in the finite strain elastic case [6, 7]. Although it is true that some time-dependent constitutive equation describes such a relationship, the form of the equation depends on specimen geometry, phase distribution, history, and is at present unknown. Additionally, cracking accompanies deformation in many cases, and no satisfactory mathematical criterion for crack initiation has yet been developed. Therefore, in order to avoid confusion, the term *rarefaction* will be used to describe features which increase in size (analogous to undergoing a tensile strain), and the term *compaction* will be used to describe features which decrease in size (analogous to undergoing a compressive strain).

## 3. Description of DMT

There are five steps to the DMT, which systematically computes the average deformations in each pixel of a digital image of a microstructure.

### 3.1. Step 1: Image acquisition

The DMT requires two digital images, one taken before deformation (the *reference image*) and one taken after deformation (the *deformed image*). As mentioned earlier, a variety of sources and magnifications for obtaining the digital images may be used. The DMT is equally applicable to digital images of a bridge or dam, or an environmental scanning electron micrograph of a few grains of cement. Likewise, the source of deformation is irrelevant, with the most likely sources being mechanical, thermal, and environmental stresses, although processes such as deterioration over longer periods of time may also be analyzed. Thus, the DMT can be used with virtually any imaging technique. As will be discussed later, the success of the technique does depend on the sharpness of the image and on the size of features within the image. Each image is stored digitally as an array of gray scales where 255 represents white and 0 represents black. These reference and deformed images must be taken at the same magnification, however, or the analysis becomes invalid.

### 3.2. Step 2: Calculation of displacements via IIMT

The second step is to use the DMT to calculate the $x_1$ and $x_2$ displacements of a search window and assign these displacements to a point. While this technique is described in detail elsewhere [1] for computing displacement between points, it is reviewed below because, for the first time, it is being applied to displacements between associated pixels, and this demands careful analysis of the resolution and reliability of the technique.

To minimize differences in brightness and contrast between the two images due to instrumentation, the intensities of the pixels in each region of analysis, referred to as a window, are modified to a distribution with a mean of zero and a standard deviation of one. From the deformed image, a small square window, 20 pixels on a side (already determined to be a useful size [1]), is centered on the pixel of interest. This window is referred to as the *search window*. A larger square window, 40 pixels on a side, is centered on the same pixel in the reference image and is called the *reference window*. The search window is systematically moved and distorted over the reference window and a minimum mean square error criterion is determined from the following:

$$\text{Minimum of } \int_{\text{Search Window}} (\text{Intensity}_{\text{search window}} - \text{Intensity}_{\text{reference window}})^2 \qquad (1)$$

The center of the search window defines a displacement. Repetition of this process determines the displacement of each pixel of the image of deformed material. Edge effects are removed by not analyzing the 40 pixels nearest each edge of both images.

In simple terms, this technique finds the location of the search window that minimizes the difference in intensity between this window and the reference window, in a least squares manner. This approach finds minimums for differences in intensity and is analogous to many finite element or finite difference techniques, where minimums in energy are sought. In all cases, the minimum may not be sharply defined, but it is unique and nontrivial.

The DMT technique has conceptual similarities to the Moire method of determining surface strains [8–10]. In the Moire technique, a grid is laid down on the undeformed sample, using lithographic or other means. After deformation, the deformed grid is compared optically with the undeformed grid. Optical interference between the two grids produces fringes, which can then be analyzed to produce surface displacements and deformations. In a sense, the DMT is a Moire technique, where the grid used is the digital image pixel structure. However, the pixel grid is always undeformed, but the changing pixel intensities are analyzed to compute local displacements and deformations. A good conceptual review of the Moire technique, as of 1970, is given in Ref. [8], while more modern developments can be found in Refs. [9] and [10].

The accuracy of the location of each center point is important. It has been reported previously [1] that the displacement of a sharp boundary between the regions of different levels of gray can be determined to an accuracy of 0.2 of a pixel in one direction (This is possible because of interpolation between rows or columns). In other words, if one pixel in each row or column were to move 0.2 of a pixel, then the 20 × 20 pixels will detect this displacement. Since twenty pixels are located with an accuracy of 0.2 pixels, the uncertainty in the location of each pixel is 0.01 pixel. The best demonstration of this is to calibrate the technique using images of known deformation, as discussed later.

### 3.3. Step 3: Calculation of deformations

When the DMT has finished operating on all pixels in the image, an array of displacements of each pixel relative to the undeformed image has been determined. The problem now is to compute local displacements, i.e. displacements relative to near neighbor displacements and not relative to the reference which for any one displacement is cumulative. So far the array of displacements represents the average displacements of the pixel centers, the location of which is not exactly defined. To calculate the deformation of each pixel, we must transfer the displacements to the pixel corners, which will serve as nodes for the finite element analysis. This is accomplished by computing the average of the displacements of four adjacent pixels as shown in Fig. 1 and defining that as the displacement of node. The $u_1$ and $u_2$ displacements of node 1, shown in Fig. 1, is given by the average of the displacements of pixels A, B, C and D according to:

$$u_1^1 = \frac{1}{4}\left(u_1^{\mathrm{A}} + u_1^{\mathrm{B}} + u_1^{\mathrm{C}} + u_1^{\mathrm{D}}\right) \tag{2a}$$

$$u_2^1 = \frac{1}{4}\left(u_2^{\mathrm{A}} + u_2^{\mathrm{B}} + u_2^{\mathrm{C}} + u_2^{\mathrm{D}}\right) \tag{2b}$$

where $u^1$ is the displacement at node 1, and $u^{\mathrm{A}}$, $u^{\mathrm{B}}$, $u^{\mathrm{C}}$, $u^{\mathrm{D}}$ are displacements of surrounding pixels. The subscripts indicate the direction of displacement, and the superscripts indicate the location of the displacement. Repetition defines an array of displacements of nodes.

The deformation (mathematically equivalent to the finite strain) tensor at a given node is defined by [5–7]:

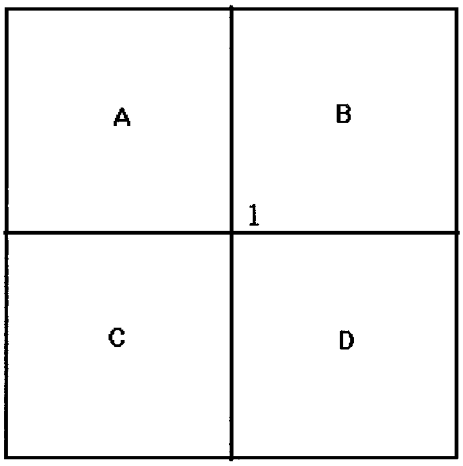

*Figure 1* Portion of finite element grid. Displacements at node 1 are calculated by averaging displacements of pixels A, B, C, and D.

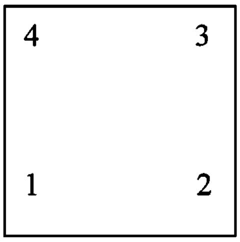

*Figure 2* Repetition of the algorithm described in Fig. 1 is used to define the displacements at the corners (nodes) of newly defined unit pixel node assignments used for deformation calculations.

$$\phi_{ik} = \frac{1}{2}\left(\frac{\partial u_i}{\partial x_k} + \frac{\partial u_k}{\partial x_i} + \frac{\partial u_l}{\partial x_i}\frac{\partial u_l}{\partial x_k}\right) \quad i, k, l = 1, 2 \tag{3}$$

where $\phi_{ik}$ is the deformation tensor, and $x$ is an arbitrary length in the direction noted by the subscript. The superscript denoting the node has been dropped for the moment. This is the full finite strain (deformation) tensor, and has not been linearized for small deformations. It is necessary to use the full finite strain form because local deformations in a microstructure can be large, especially when cracking or de-bonding takes place, as mentioned previously. The three independent (two diagonal, one off-diagonal) elements of the deformation tensor are:

$$\phi_{11} = \frac{1}{2}\left[2\frac{\partial u_1}{\partial x_1} + \left(\frac{\partial u_1}{\partial x_1}\right)^2 + \left(\frac{\partial u_2}{\partial x_1}\right)^2\right] \tag{4a}$$

$$\phi_{22} = \frac{1}{2}\left[2\frac{\partial u_2}{\partial x_2} + \left(\frac{\partial u_1}{\partial x_2}\right)^2 + \left(\frac{\partial u_2}{\partial x_2}\right)^2\right] \tag{4b}$$

$$\phi_{12} = \frac{1}{2}\left[\frac{\partial u_1}{\partial x_2} + \frac{\partial u_2}{\partial x_1} + \frac{\partial u_1}{\partial x_1}\frac{\partial u_1}{\partial x_2} + \frac{\partial u_2}{\partial x_1}\frac{\partial u_2}{\partial x_2}\right] \tag{4c}$$

To compute these deformations, it becomes necessary to describe the displacements as functions of $x_1$ and $x_2$, so that the derivatives indicated in Equations 4a–c can be determined. It is possible to approximately describe the displacement at any point along a given direction as a function of $x_1$ and $x_2$, $0 < x_1, x_2 < 1$ (origin at node 1), through simple linear interpolation formulae, by treating the new "deformed pixel" as a bi-linear finite element [11–13]:

$$u_1(x_1, x_2) = (1 - x_1)(1 - x_2)u_1^1 + x_1(1 - x_2)u_1^2 + x_1x_2u_1^3 + (1 - x_1)x_2u_1^4 \tag{5a}$$

$$u_2(x_1, x_2) = (1 - x_1)(1 - x_2)u_2^1 + x_1(1 - x_2)u_2^2 + x_1x_2u_2^3 + (1 - x_1)x_2u_2^4 \tag{5b}$$

where the superscripts 1, 2, 3, and 4 represent the four corners of the new pixels, each corner being a node (The superscripts are as defined for Equation 2). These formulae can be used to evaluate Equation 4a–c, resulting in the following:

$$\phi_{11} = \frac{1}{2}\left(k_1x_2^2 + k_2x_2 + k_3\right) \tag{6a}$$

$$\phi_{22} = \frac{1}{2}\left(k_4x_1^2 + k_5x_1 + k_6\right) \tag{6b}$$

$$\phi_{12} = \frac{1}{2}(k_7x_1 + k_8x_2 + k_9x_1x_2 + k_{10}) \tag{6c}$$

where

$$k_1 = \left[\left(u_1^2 - u_1^1\right) - \left(u_1^3 - u_1^4\right)\right]^2 + \left[\left(u_2^2 - u_2^1\right) - \left(u_2^3 - u_2^4\right)\right]^2 \tag{7a}$$

$$k_2 = 2\left[\left(u_1^3 - u_1^4\right) - \left(u_1^2 - u_1^1\right) - \left(u_1^2 - u_1^1\right)^2 + \left(u_1^2 - u_1^1\right)\left(u_1^3 - u_1^4\right) - \left(u_2^2 - u_2^1\right)^2 + \left(u_2^2 - u_2^1\right)\left(u_2^3 - u_2^4\right)\right] \tag{7b}$$

$$k_3 = 2\left(u_1^2 - u_1^1\right) + \left(u_1^2 - u_1^1\right)^2 + \left(u_2^2 - u_2^1\right)^2 \tag{7c}$$

$$k_4 = \left[\left(u_1^4 - u_1^1\right) - \left(u_1^3 - u_1^2\right)\right]^2 + \left[\left(u_2^4 - u_2^1\right) - \left(u_2^3 - u_2^4\right)\right]^2 \tag{7d}$$

$$k_5 = 2\left[\left(u_2^3 - u_2^2\right) - \left(u_2^4 - u_2^1\right) - \left(u_2^4 - u_2^1\right)^2 + \left(u_2^4 - u_2^1\right)\left(u_2^3 - u_2^2\right) - \left(u_1^4 - u_1^1\right)^2 + \left(u_1^4 - u_1^1\right)\left(u_1^3 - u_1^2\right)\right] \tag{7e}$$

$$k_6 = 2\left(u_2^4 - u_2^1\right) + \left(u_1^4 - u_1^1\right)^2 + \left(u_2^4 - u_2^1\right)^2 \tag{7f}$$

$$k_7 = \left(u_1^3 - u_1^2\right) + \left(u_1^2 - u_1^1\right)\left(u_1^3 - u_1^2\right) + \left(u_2^2 - u_2^1\right)\left(u_2^3 - u_2^2\right) - \left(u_1^4 - u_1^1\right) - \left(u_1^2 - u_1^1\right)\left(u_1^4 - u_1^1\right) - \left(u_2^2 - u_2^1\right)\left(u_2^4 - u_2^1\right) \tag{7g}$$

$$k_8 = \left(u_2^3 - u_2^4\right) + \left(u_1^3 - u_1^4\right)\left(u_1^4 - u_1^1\right) + \left(u_2^3 - u_2^4\right)\left(u_2^4 - u_2^1\right) - \left(u_2^2 - u_2^1\right) - \left(u_1^2 - u_1^1\right)\left(u_1^4 - u_1^1\right) - \left(u_2^2 - u_2^1\right)\left(u_2^4 - u_2^1\right) \tag{7h}$$

$$k_9 = \left(u_1^2 - u_1^1\right)\left(u_1^4 - u_1^1\right) + \left(u_1^3 - u_1^2\right)\left(u_1^3 - u_1^4\right) + \left(u_2^2 - u_2^1\right)\left(u_2^4 - u_2^1\right) + \left(u_2^3 - u_2^2\right)\left(u_2^3 - u_2^4\right) - \left(u_1^2 - u_1^1\right)\left(u_1^3 - u_1^2\right) - \left(u_1^3 - u_1^4\right)\left(u_1^4 - u_1^1\right) - \left(u_2^2 - u_2^1\right)\left(u_2^3 - u_2^2\right) - \left(u_2^3 - u_2^4\right)\left(u_2^4 - u_2^1\right) \tag{7i}$$

$$k_{10} = \left(u_1^4 - u_1^1\right) + \left(u_2^2 - u_2^1\right) + \left(u_1^2 - u_1^1\right)\left(u_1^4 - u_1^1\right) + \left(u_2^2 - u_2^1\right)\left(u_2^4 - u_2^1\right) \tag{7j}$$

The average deformation for the new pixel (area within four nodes) is computed by integrating over the entire pixel via:

$$\langle\phi\rangle = \frac{1}{2}\int_0^1\int_0^1 \mathrm{d}x_1\,\mathrm{d}x_2\phi(x_1, x_2) \tag{8}$$

The equations for the finite strain tensor are:

$$\langle\phi_{11}\rangle = \frac{1}{2}\left(\frac{k_1}{3} + \frac{k_2}{2} + k_3\right) \tag{9a}$$

$$\langle\phi_{22}\rangle = \frac{1}{2}\left(\frac{k_4}{3} + \frac{k_5}{2} + k_6\right) \tag{9b}$$

$$\langle\phi_{12}\rangle = \frac{1}{2}\left(\frac{k_7}{2} + \frac{k_8}{2} + \frac{k_9}{4} + k_{10}\right) \tag{9c}$$

The $x_1$ and $x_2$ dependence of the deformation within the pixel is not meaningful, since the pixel is the smallest material unit.

The diagonalized deformation tensor gives the principal deformations within each pixel. To find the eigenvalues, or principal deformations, for the tensor, it is necessary to solve Equation 10 using $\langle\phi\rangle$ from Equation 9:

$$\begin{vmatrix} \langle\phi_{11}\rangle - \lambda_1 & \langle\phi_{12}\rangle \\ \langle\phi_{12}\rangle & \langle\phi_{22}\rangle - \lambda_2 \end{vmatrix} = 0 \tag{10}$$

where λ = the eigenvalues. The resulting solutions take the form:

$$\phi_{11}^*, \phi_{22}^* = \frac{(\phi_{11} + \phi_{22}) \pm \sqrt{\left[(\phi_{11} + \phi_{22})^2 - 4\left(\phi_{11}\phi_{22} - \phi_{12}^2\right)\right]}}{2} \tag{11}$$

where $\phi_{11}^*$ and $\phi_{22}^*$ are the principal deformations averaged over the given pixel. This ability to compute principal deformations, as opposed to simple displacements, makes this technique unique.

### 3.4. Step 4: Filtering the deformation map

A median filter was used to remove the background noise from the deformation map. This is a simple filter, which eliminates very high and very low values from the analysis, which are usually spurious noise generated by the algorithm [14]. It operates on each pixel in the deformation map sequentially. The deformation values of the current pixel and the eight surrounding pixels are ranked by magnitude, and the median value of that ranking is assigned to the current pixel. It is important to note that this new value is stored in a different map, so that all of the filter analysis is performed on the original data set, rather than a combination of original and filtered data. The final deformation map is then represented by the filtered data set.

### 3.5. Step 5: Reporting the data

The results of this analysis can be presented in several formats. First, the deformations in each pixel can be mapped to allow direct comparison between high deformation areas and their associated microstructural features. At present, most of the deformation maps, including all of the deformation maps shown in this paper, report average linear deformation based on area shrinkage or swelling for each pixel. This is determined by calculating the fractional area change in a pixel and taking the square root by:

$$\phi = \frac{\Delta l}{l} = \sqrt{a_{\text{final}} - a_{\text{initial}}} \qquad (12)$$

where $l = 1$, the unit pixel length; $a_{\text{final}} = (1 + \phi^*_{11})(1 + \phi^*_{22})$; and $a_{\text{initial}} = 1$. Additional maps consisting of each component of the deformation tensor, $\phi_{11}$, $\phi_{22}$, and $\phi_{12}$, or of the principal deformations, $\phi^*_{11}$ and $\phi^*_{22}$ can be created using Equations 9a–c or 11, respectively. There are two kinds of maps commonly used in this work: a compaction map and a rarefaction map. In a compaction map, all areas with positive deformations are turned to white, and the areas with compaction deformation are scaled so that the darker the gray scale, the higher the magnitude of the compaction. The rarefaction maps are similarly constructed, with all pixels with negative deformations turned white, and the positive deformations scaled so that the darker the gray scale, the higher magnitude the deformation.

From a given map, deformation distributions can be constructed to illustrate the numerical distribution of deformations in a sample. These are constructed by counting the number of pixels with a given average linear deformation and representing the data as a histogram of area fraction vs. deformation. The distribution gives quantitative information about local deformations in the microstructure. Integrating the deformation distribution gives the total deformation of the image.

## 4. 2-D vs. 3-D considerations

As with most microscopic techniques and also most techniques for measuring strain, information is obtained from a surface, which is less constrained than the interior. This is particularly important to keep in mind when measuring local deformation, and particularly so on a rough surface where constraints could be very different than they would be in the interior. In spite of shortcomings such as this, the DMT can provide useful insights about deformation within the microstructure of complex materials.

Another possible point of concern in the IIMT part of the DMT is the use of 2-D images to represent the 3-D mechanisms occurring during deformation. This topic has been covered in detail in other papers [3] but will be repeated here due to its importance.

In previous work [3, 4], the samples used were fracture flakes, approximately 1 mm thick, and about 1 cm$^2$ in area. These were approximately unrestrained in all three dimensions. The shape of the samples implies that, if we were to think of them as 2-D samples, we should use the plane stress conditions, which is more applicable to thin samples [15]. The IIMT technique measures the shrinkage deformation in two dimensions only.

An examination of the physical situation being studied confirms the applicability of this technique. Take, for example, a shrinking layer that surrounds a single nonshrinking particle such as shown in cross-section in Fig. 3a. The fracture plane labeled in the figure is the average surface of the sample, with the particle:product composite protruding above the fracture plane. The outer circle (labeled *Before shrinkage*) indicates the

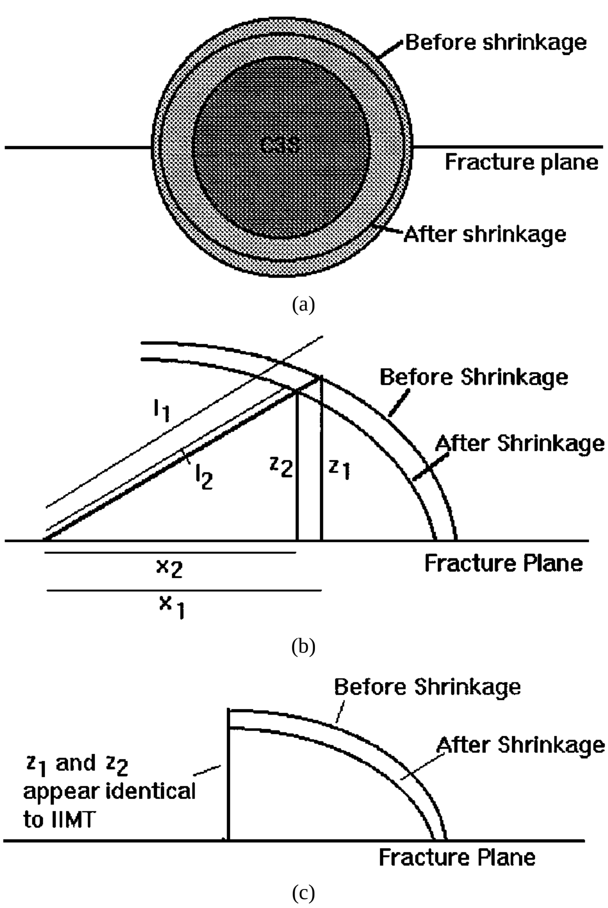

(a)

(b)

(c)

*Figure 3* (a) Example of particle surrounded by shrinking phase protruding above the fracture plane (sample surface) showing outer radius before and after shrinkage (Dark gray = particle; Light gray = shrinking phase); (b) Similar triangles created by shrinkage shown in (a); (c) Representation of singularity for points lying directly above the center of the particle.

outer limits of the product in a wet state; the inner circle (labeled *After shrinkage*) indicates the new product limit as drying shrinkage occurs. Assuming this shrinkage at this scale is homogeneous and isotropic, a pair of similar triangles may be drawn from the center of the particle to any point on its outer edge, as shown in Fig. 3b. For similar triangles, it is known that:

$$\frac{l_1}{l_2} = \frac{x_1}{x_2} \tag{13}$$

indicating that the projection of the outer radius (the $x$'s) will scale directly with the change in length of the the outer radius (the $l$'s). More explicitly, the deformation along the $l$-direction is given by:

$$\phi_l = \frac{l_2 - l_1}{l_1} \tag{14}$$

Similarly, the deformation along the $x$-direction is given by:

$$\phi_x = \frac{x_2 - x_1}{x_1} \tag{15}$$

Re-arranging Equation 13, and substituting into Equation 15 gives:

$$\phi_x = \frac{x_2 - \frac{l_1}{l_2}x_2}{\frac{l_1}{l_2}x_2} = \frac{l - \frac{l_1}{l_2}}{\frac{l_1}{l_2}} = \frac{l_2 - l_1}{l_1} = \phi_1 \tag{16}$$

Thus, the deformation along the $x$-direction is identical to that in the $l$-direction. We only report $x_1$, $x_2$ deformations, and any out of plane deformations are not part of the analysis.

What if the layers re-arrange or move without shrinking? This is possible, but highly unlikely within the product of cement hydration, except on a very small scale due to the densely layered nature of the shrinking product [16, 17]. The interlayer distances in C-S-H are on the nanometer scale, providing very little room for movement of a single layer. It is comparable to moving one page in a closed book. However, at the larger scale, shifting or crumpling particles could account for very large apparent deformation at the edge of the particle or at the edge of an opening crack. The problems must be considered when interpreting IIMT and DMT.

## 5. Experimental accuracy of the DMT

The deformation at each pixel is computed in such a way that information is taken from many pixels and then the average deformation of nearest neighbors is incorporated into the final result for the area of each pixel. The mathematical accuracy of DMT has not been determined analytically, so it is useful to experimentally explore the accuracy of the technique, which will also serve to validate the technique.

The validity and accuracy of the DMT was assessed by comparison of DMT results with a numerically "exact" solution determined by a finite element model.

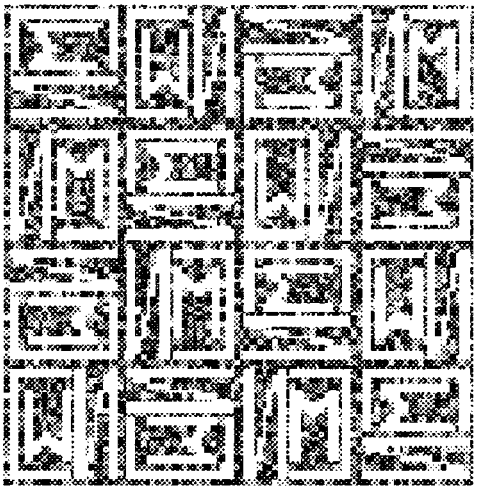

*Figure 4* Initial 100 × 100 pixel version of model microstructure for DMT reference image. The initials 'CMN' are white with random gray levels in the background.

The idea is to use an established finite element technique [12, 13], applied to a model microstructure to 1) compute the average (linear elastic) deformations across the microstructure, where some of the phases were shrinking and some were restraining, and 2) produce a deformed image to which the DMT could be applied. The resulting deformations computed by the DMT could then be quantitatively compared to the deformations computed by the finite element technique, which is known to be accurate [12, 13].

A 100 × 100 pixel model microstructure was constructed as shown in Fig. 4. The reason for the small size of the image, i.e. less than 500 × 500 pixels, will become apparent shortly. The model microstructure consisted of the letters "CMN" aligned in various directions. Each pixel within the initials was assigned a greyscale value of 255 (pure white). The letters occupy 4,720 of the 10,000 pixels, for an area fraction of 47.2%. Each pixel in the background was assigned a random greyscale value between 0 and 254 in order to give a wide range of greyscales for the IIMT to operate on. This is required, as the IIMT can operate on a simple two phase image, but if only one sharp boundary moves, all of the pixels will be moved without any influence from the others which have only a constant level of gray and therefore do not influence the least squares' minimization process (i.e. all displacements have the same influence). If there is detail, however, within the search window, the minimization process will fairly incorporate all of the pixels as it seeks a well-defined minimum. Without the detail, there will be a tendency to overestimate average displacements because of the domination of a few pixels.

A finite element technique specialized for digital images [12,13] was used to simulate free shrinkage on the model microstructure. For this simulation, the image was treated as consisting of only two regions which we will call phases, as shown in Fig. 5. One phase consisted of the pixels with a single greyscale of 255 (the initials); the other phase consisted of all of the pixels with a greyscale between 0 and 254 (the background).

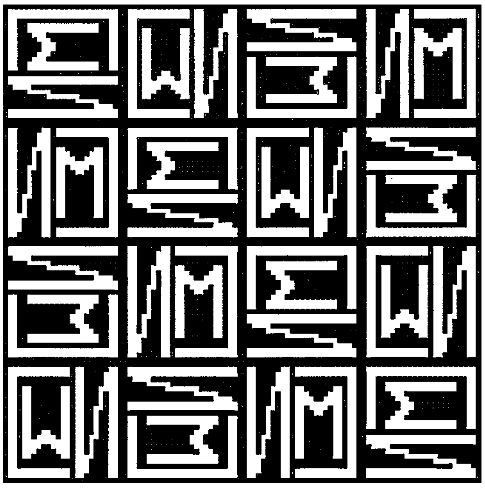

*Figure 5* The initials 'CMN' are white, and the background black for the 100 × 100 pixel model microstructure used for finite element simulation of shrinkage.

Again the initials occupied an area fraction of 47.2% (4,720 of 10,000 pixels). In one respect, this is a fairly severe test of the DMT because it will work better if the initials phase contained detail. The "initials" phase was assigned an elastic modulus three times that of the background phase ($E_{\text{initials}}/E_{\text{background}} = 3$), and was assigned an intrinsic shrinkage of 10%. This means that the "initials" phase would shrink 10% in each direction if left in an unrestrained state. The background phase was assumed to be a non-shrinking, restraining phase. After running the finite element simulation, the computed displacements at each node in the 100 × 100 pixel image were used to compute the average strain, or deformation, in each pixel.

Two larger microstructures, 500 pixels square, were then produced to provide higher resolution images needed for this test of the accuracy of the DMT. The first of these two microstructures was simply a scale-up of the undeformed microstructure shown in Fig. 4. This microstructure was computed by mapping each pixel in the 100 × 100 pixel microstructure onto the corresponding $5 \times 5 = 25$ pixels in the 500 × 500 pixel microstructure, as shown in Fig. 6. The resulting microstructure is identical to the initial model microstructure except in the number of pixels it contains. This served as the *reference image* used for testing the DMT.

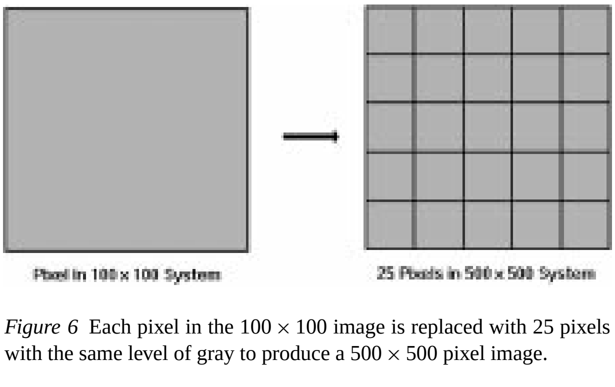

*Figure 6* Each pixel in the 100 × 100 image is replaced with 25 pixels with the same level of gray to produce a 500 × 500 pixel image.

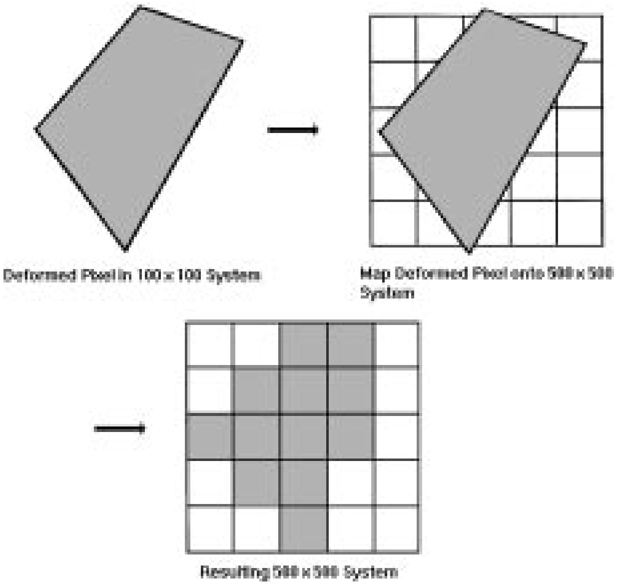

*Figure 7* The computed deformed pixel (a) is simulated by overlaying the deformed pixel on a 5 × 5 pixel square and (b) converting all pixels that are more than half covered to the appropriate level of gray (c).

The next image needed is an image of a deformed microstructure upon which the DMT will operate. To obtain this image, a third microstructure used the displacements calculated by the shrinkage simulation on the 100 × 100 pixel system to calculate the actual new shape of each pixel in the 500 × 500 pixel microstructure. This is the main reason why the initial image was 100 × 100, as the scaling to 500 × 500 facilitates producing the effect of deformed pixels with the use of standard pixels particularly when the deformation is not rectilinear as shown in Fig. 7. A 500 × 500 pixel image was then used to display these new, deformed shapes that were computed at 100 × 100 resolution. This process is demonstrated in Fig. 7, where the five times higher resolution is used to show the new shape of the model microstructure. In conjunction with the scaled up undeformed images, the DMT uses the microstructure shown in Fig. 8, the *deformed image*, to compute deformation. This process was carried out in order to produce a deformed image similar to that seen in a microscope.

Finally a microstructure of the computed deformations, for comparison, with DMT measured deformations, was produced. The microstructure was a scale up of Fig. 5, produced as above, to 500 × 500 pixels. The finite element simulation was then re-run at this resolution, giving a 500 × 500 pixel image of the average deformations in each pixel. The result of the DMT, which is a 500 × 500 pixel deformation map, will be *compared* to this image of deformations.

Fig. 8 shows the rarefaction map for the 500 × 500 pixel images: (a) finite element solution, and (b) DMT technique, and Fig. 9 shows the corresponding compaction maps. As can be seen, there are some areas of higher deformation that are detected in the DMT analysis but are not present in the exact solution analysis. This is probably due to local lack of detail in the letters as already described. Overall, the agreement

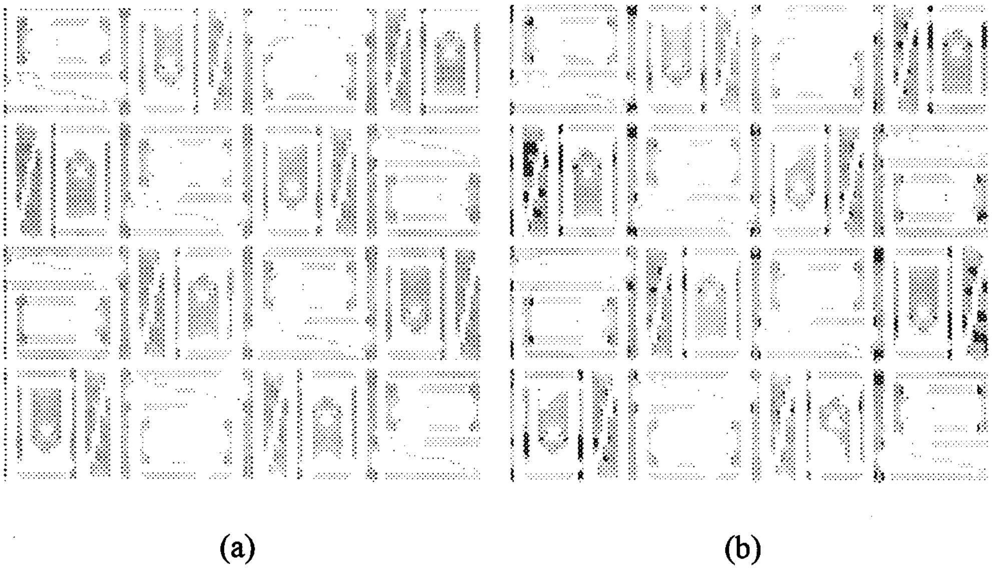

*Figure 8* Comparison of compaction maps between (a) finite element solution, and (b) DMT technique. Darker colors indicate higher magnitude deformations.

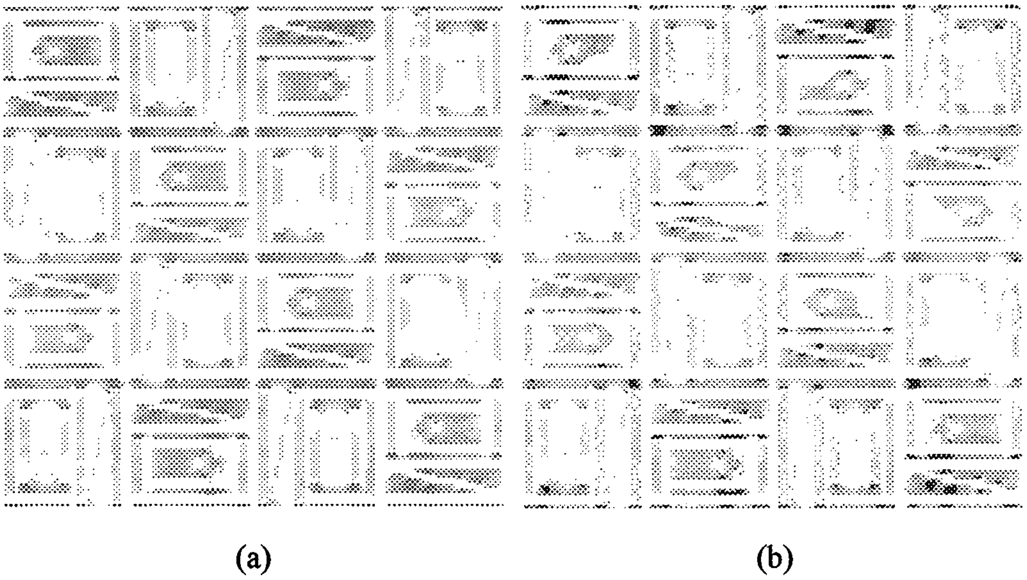

*Figure 9* Comparison of rarefaction maps between (a) finite element solution, and (b) DMT technique. Darker colors indicate higher magnitude deformations.

between the exact solution and the DMT technique seems at least qualitatively good.

Fig. 10 shows histograms of deformation (i.e. number of pixels at each deformation) as determined both by the finite element simulation and the DMT, for both compaction and rarefaction. The agreement between the two methods is excellent, which demonstrates the quantitative accuracy of the DMT. The small disagreement at higher magnitude deformation from the higher deformations in Figs 8 and 9 may be partly due to few high deformations incorrectly determined by the DMT, and possibly, also by the fact that the DMT used the full finite strain defined in terms of the displacements, Equation 3, while the finite element simulation used a linearized form of Equation 3 [12,13]. The DMT accurately reproduces the double peak shown in the numerical solution. In real random microstructures, the double peak, here attributable to having two phases, is usually merged, because of randomness, into a single broad peak.

## 6. Effects of scale

The DMT can be applied to different magnification views of the same area in a microstructure. It has been shown previously that, if the image is scale invariant, so that it looks the same at different magnifications, then the DMT gives the same result for deformations [3] at each scale. However, the composite microstructures of cement-based materials are not invariant over the range of magnification usually used by scanning electron microscope studies.

In cement paste, one could presumably focus on just the gel phases, or go to lower magnification and include unhydrated cement and crystalline phases as well. In that case, changing the magnification also changes the

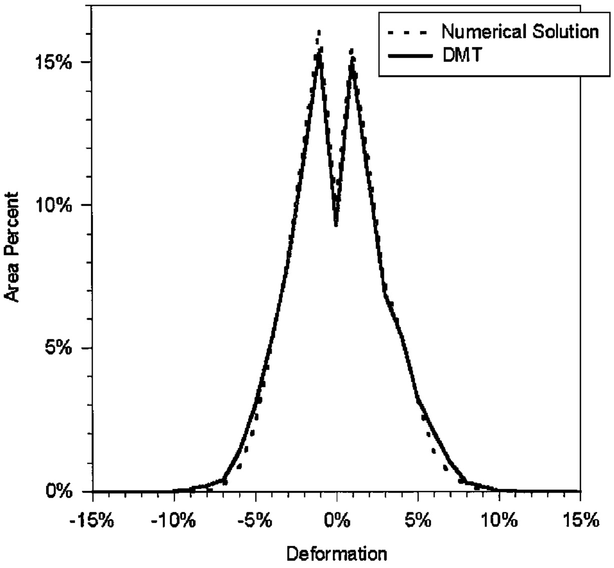

*Figure 10* Comparison of deformation distributions for finite element solution (- - -) and DMT (—) computed deformations.

part of the microstructure viewed, and so the DMT will give, in general, different results at different magnifications, as it should if the microstructure is not scale invariant.

Another procedure would be to use lower magnification, but then run the DMT on the part of the image viewed at higher magnification. This would give the same result except that the DMT requires fine scale contrast. Good use of DMT requires judgments about resolution and field of view, as does any microscopic technique.

## 7. Summary

A new deformation mapping technique (DMT) has been described, capable of mapping deformations associated with each pixel in a microstructure. The technique is insensitive to the image source or the source of deformation. It requires two digital images: a reference image, taken before deformation occurs; and a deformed image, taken after deformation. Computer algorithms are used to analyze the displacements between these two images for each pixel in the microstructure. These displacements are then used to calculate the principal (normal) deformations, which are used to compute the average deformation in each pixel. There are a number of analytical steps that interpolate information from near neighbor pixels and so facilitate a highly accurate result. The results can be presented as either a deformation map, a distribution of deformations, or as a data file. Comparison of the DMT run on a simulated microstructure with corresponding exact solutions using finite element analysis shows that the accuracy of this technique is good. The next paper in this series [18] utilizes this image intensity matching technique to analyze the drying shrinkage deformations that develop in a variety of cement pastes.

## Acknowledgements

The authors gratefully acknowledge the financial support provided by the U.S. Department of Energy (Award CE-FG02-91ER45460). C. M. N. wishes to thank the Department of Defense for funding via a National Defense Science and Engineering Graduate Fellowship.

## References

1. Y. XI, T. B. BERGSTROM and H. M. JENNINGS, *Comput. Mater. Sci.* **2** (1994) 249.
2. T. B. BERGSTROM, PhD Thesis, Northwestern University, 1993.
3. C. M. NEUBAUER, T. B. BERGSTROM, K. SUJATA, Y. XI, E. J. GARBOCZI and H. M. JENNINGS, *J. Mat. Sci.* **32** (1997) 6415.
4. C. M. NEUBAUER, H. M. JENNINGS and E. J. GARBOCZI, *Cem. Con. Res.* **27**(10) (1997) 1603.
5. L. D. LANDAU and E. M. LIFSHITZ, "Theory of Elasticity" (Pergamon Press, Oxford, 1986).
6. D. C. WALLACE, *Phys. Rev.* **162** (1967) 776.
7. R. N. THURSTON, *J. Acoust. Soc. Amer.* **37** (1965) 348.
8. A. J. DURELLI and V. J. PARKS, "Moire Analysis of Strain" (Prentice-Hall, Englewood Cliffs, New Jersey, 1970).
9. J. C. DUPRE, M. COTTRON and A. LAGARDE, *Exp. Mech.* **35** (1995) 153.
10. B. HAN, P. IFJU and D. POST, *ibid.* **33** (1993) 195, 349.
11. R. D. COOK, D. S. MALKUS and M. E. PLESHA, "Concepts and Applications of Finite Element Analysis" (John Wiley & Sons, New York, 1989).
12. E. J. GARBOCZI and A. R. DAY, *J. Mech. Phys. Solids* **43** (1995) 1349.
13. E. J. GARBOCZI, NIST Internal Report 6394, United States Department of Commerce, National Institute of Standards and Technology, Gaithersburg, MD, 1998. Also available at http://ciks.cbt.nist.gov/garboczi/, Chapter 2.
14. K. R. CASTLEMAN, "Digital Image Processing" (Prentice-Hall, Englewood Cliffs, N.J., 1979).
15. J. W. EISCHEN and S. TORQUATO, *J. Appl. Phys.* **74**(1) (1993) 159.
16. R. F. FELDMAN and P. J. SEREDA, *Mater. Struct.* **1** (1968) 509.
17. *Idem., Eng. J.* **53** (1970) 53.
18. C. M. NEUBAUER and H. M. JENNINGS, *Journal of Materials Science*, submitted.

*Received 14 July 1998*
*and accepted 31 March 2000*